Slope Valleys

ACCOMMODATION CHANGE DURING BYPASS ACROSS A LATE-STAGE FAN IN THE SHALLOW AUGER BASIN

CHARLES W. BOHN IV
The Pennsylvania State University, University Park, Pennsylvania 16802, U.S.A.
Present address: Shell Exploration and Production Company, 200 N. Dairy Ashford, Houston, Texas 77079, U.S.A.
e-mail: charles.bohn@shell.com
PETER B. FLEMINGS
University of Texas at Austin, 1 University Station C1100, Austin, Texas 78712-0254, U.S.A.
e-mail: pflemings@jsg.utexas.edu
AND
RUDY L. SLINGERLAND
The Pennsylvania State University, 513A Deike Building, University Park, Pennsylvania 16802, U.S.A.
e-mail: sling@geosc.psu.edu

Abstract: Apron 1 in the Shallow Auger Fan System records the transition from ponded deposition in the lobe complex to bypass at the top of the channel complex. The lobe complex, at the base of Apron 1, exhibits characteristics typical of ponded apron deposits: it onlaps the basin margin, exhibits a concentric isopach pattern, has a lobe geometry in amplitude extraction, and is composed of continuous seismic reflections that have uniform thickness. The transition from ponded deposition to bypass is recorded with increasing gradients along the four channels in the channel complex. Healed-slope accommodation is filled as these channels aggrade at the sediment entry point. In the proximal reaches, the channels have thick levee deposits and minimal incision. Downdip, the levee deposit thickness decreases and incision increases. Each channel aggrades to a single gradient; once this gradient is achieved, the channel avulses to an area of greater accommodation. As healed-slope accommodation fills, channel gradients in the proximal reaches decrease and sinuosity increases. In the distal reaches of the channel, greater incision depths may compartmentalize the underlying ponded deposits.

Key Words: Shallow Auger Fan, slope accommodation, healed-slope accommodation, submarine-valley morphology

INTRODUCTION

The stratigraphic architecture of turbidite deposits in withdrawal mini-basins follows a repeatable succession (Fig. 1): initially, sediments are deposited as low-gradient sheet deposits; subsequently these deposits are overlain by sloping channelized deposits. This characteristic architecture has been described as a "ponded phase", which is overlain by a "slope healing phase" (Beaubouef and Friedmann, 2000; Booth et al., 2000; Prather, 2003; Prather et al., 1998). Analysis of this commonly observed architecture is important for a range of reasons. First, ponded deposits vs. healed-slope deposits have very different stratigraphic architectures. A better understanding of the geometry, the lithology, and the evolution of these deposits is important for optimizing petroleum production. Perhaps more fundamentally, a process-based understanding of the controls behind ponded vs. healed-slope deposition will help us to better understand deep marine sedimentation.

Sediments deposited in ponded accommodation aggrade to a horizontal surface coincident with the lowest elevation of the basin margin (Beaubouef and Friedmann, 2000; Prather, 2003; Prather et al., 1998) (Fig. 1). After this accommodation is filled, incoming flows begin to bypass the basin and proceed downslope (Sinclair and Tomasso, 2002). During the healing phase, sediments aggrade to a baselevel defined by the basin entry and basin exit points (Beaubouef and Friedmann, 2000; Prather, 2003; Prather et al., 1998).

The ponded phase is characterized by flat-lying or gently sloping deposits of alternating sand and shale that result from containment of the flow within the basin (Beaubouef et al., 2003a; Beaubouef and Friedmann, 2000; Beaubouef et al., 2003b; Toniolo et al., 2006a; Toniolo et al., 2006b). They are imaged as continuous seismic reflections onlapping the basin margin (Beaubouef and Friedmann 2000; Booth et al. 2003; Booth et al. 2000; Booth et al. 2002; Prather 2003; Prather et al. 1998; Winker and Booth 2000). These deposits have a concentric isopach map pattern that is thick in the center and thins at the margins. Ponded turbidite deposits are commonly interpreted to be formed when a long-lived turbidity current enters a basin. Under these conditions, a horizontal settling interface is maintained at a constant height by the incoming flow; this creates a deposit of uniform thickness (Hoyal et al., 2003; Toniolo et al., 2006a; Toniolo et al., 2006b; Van Wagoner et al., 2003). Imran et al. (1998) proposed a conceptual and quantitative model wherein sheet sands are deposited when the deposition rate of turbidity flows exceeds the erosion rate at all locations.

In the slope healing phase, apron deposition at the sediment entry point builds a basinward-tapering wedge (Beaubouef et al., 2003a). These aprons are convex up and exhibit an elongate isopach map pattern where the isopach thick shifts updip to the basin entry point (Mitchum, 1985; Nelson, 1984; Nilsen, 1990; Richards and Bowman, 1998; Shanmugam and Moiola, 1985). Seismic reflections range from chaotic in proximal and medial regions of the apron to downlapping, continuous sheetlike reflections in distal portions (Beaubouef et al., 2003a; Beaubouef et al.,

Application of the Principles of Seismic Geomorphology to Continental-Slope and Base-of-Slope Systems:
Case Studies from Seafloor and Near-Seafloor Analogues
SEPM Special Publication No. 99, Copyright © 2011
SEPM (Society for Sedimentary Geology), ISBN 978-1-56576-304-3, p. 219–236.

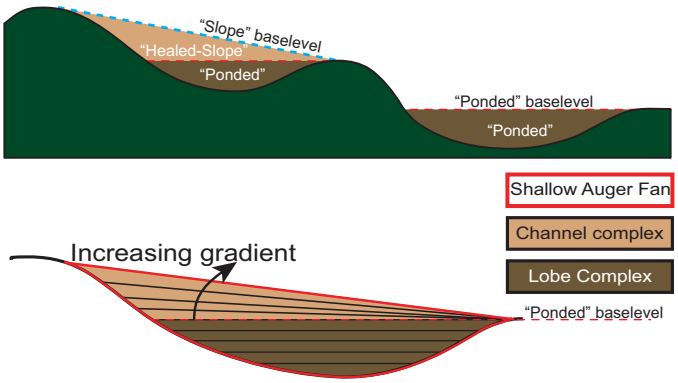

FIG. 1.—Schematic dip section and accommodation terminology. Conceptual model relating depositional gradients of a typical sequence in an idealized withdrawal mini-basin to accommodation and baselevel. Deposits in "ponded" accommodation are flat-lying or low gradient, while gradients progressively increase through deposition in the "healed-slope" accommodation. Terminology for accommodation is modified after Prather et al. (1998), and the baselevel positions are modified after Beaubouef and Freidmann (2000), Booth et al. (2000), Prather et al. (1998), and Sinclair and Tomasso (2002).

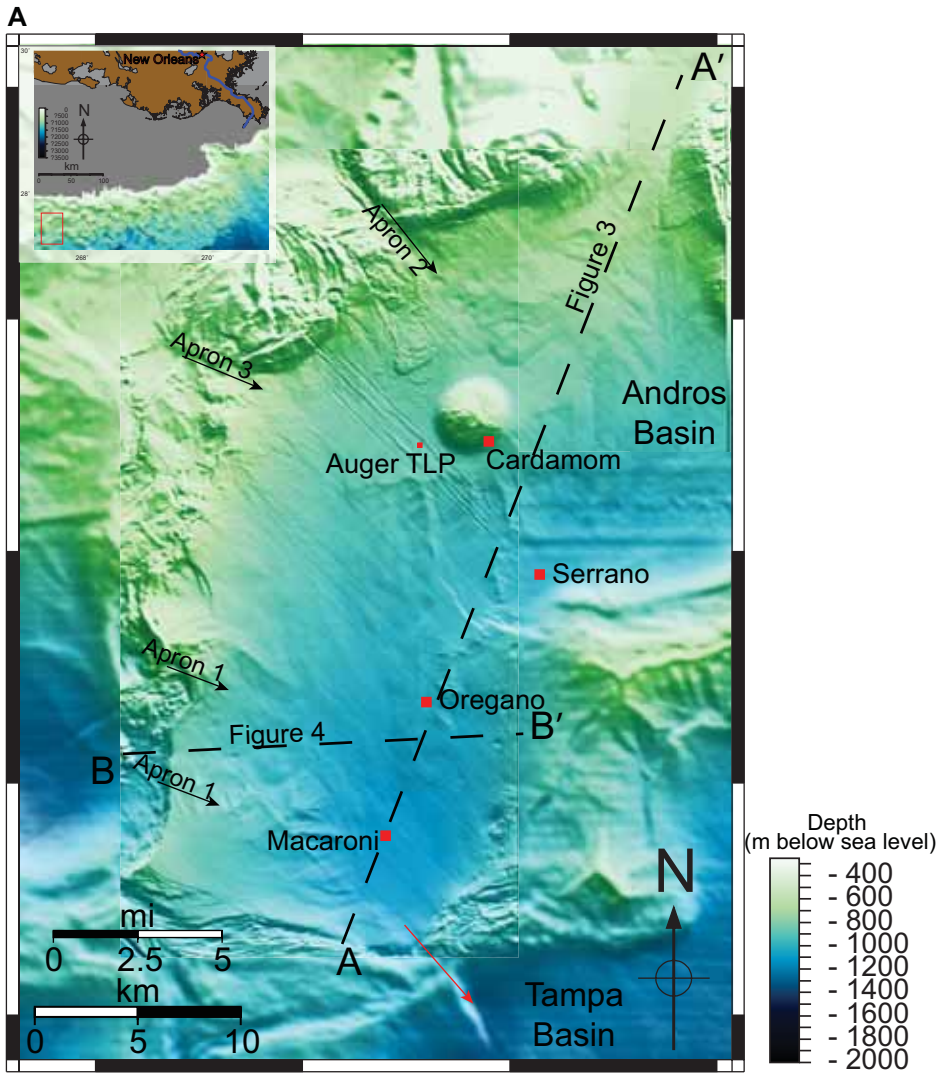

FIG. 2 (above and on facing page).—**A)** Location of the Auger Basin in the Gulf of Mexico. Seismic structure map of the seafloor overlaid on a sidelit bathymetric image of the Andros, Auger, and Tampa basins. The Auger Basin lies 345 km southwest of New Orleans, Louisiana (inset). Lines of section A–A' (Fig. 3) and B–B' (Fig. 4) are indicated with dashed lines. Black arrows indicate the source locations for Aprons 1, 2, and 3 in the Shallow Auger Fan System, and the red arrow indicates the basin exit point. Seismic image courtesy of CGGVeritas, Houston, Texas. **B)** Detail of the Shallow Auger Fan System. Color bar is thickness between the top and base of the Shallow Auger Fan System in meters (pink and light blue lines in Figure 3). The outlined areas correspond to Channels A–D (Figs. 8, 9, 11) and the location of Aprons 1, 2, and 3 that constitute the Shallow Auger Fan System. Line of section C–C' (Fig. 5) is indicated with a heavy black line. Seismic image courtesy of CGGVeritas, Houston, Texas.

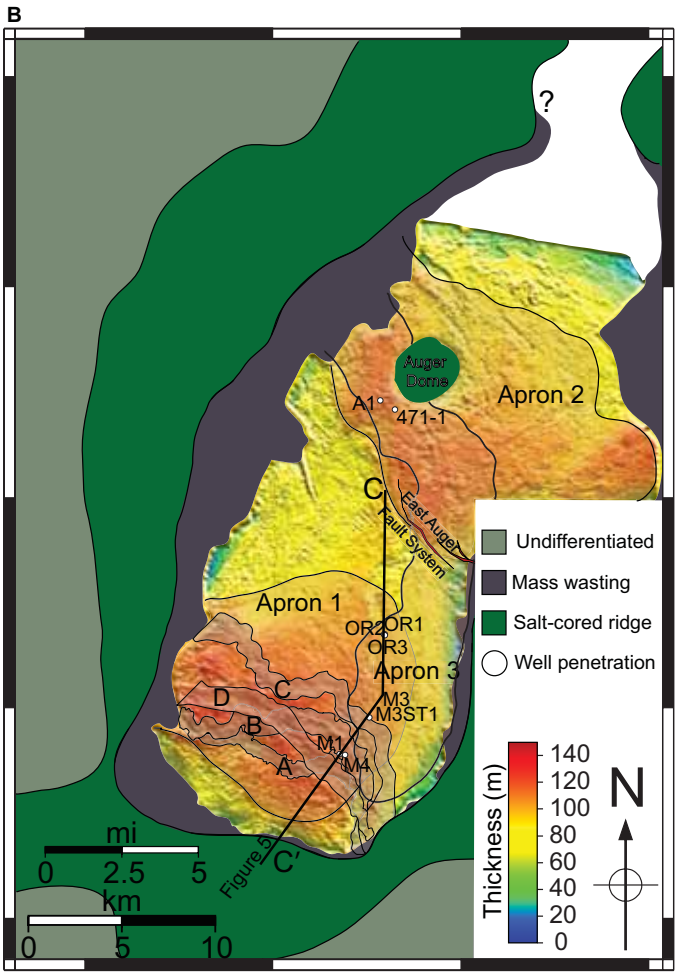

FIG. 2 (continued).—

2003b; Nilsen, 1990). Apron formation occurs when the incoming flows decelerate and spread onto the low-gradient, ponded surface, leading to rapid sedimentation proximal to the source (Beaubouef et al., 2003a; Hoyal et al., 2003; Kneller, 1999).

The transition from ponded to healed-slope deposition has been the focus of recent shallow analog studies (Barton, this volume, and Prather et al., this volume). This research takes advantage of the higher frequency of shallow seismic data in Auger Basin to document the transition from ponded deposits to healed-slope deposits in Apron 1 of the Late Pleistocene Shallow Auger Fan System (Figs. 2A, B). A range of work has taken advantage of high-frequency seismic data to study shallow depositional systems as analogs for deep reservoirs (Adeogba et al., 2005; Beaubouef et al., 2003a; Beaubouef et al., 2003b; Deptuck et al., 2003; Sawyer et al., 2007; Winker and Booth, 2000).

Apron 1 is composed of a ponded facies, the lobe complex, which is overlain by a slope facies termed the channel complex (Fig. 3). The channel complex is composed of four successive submarine valley systems (Channels A–D). The morphology of these valley systems records the growth of the channel-complex slope apron. We perform detailed analysis of these submarine valley systems to document their morphologic evolution and gradient change through the growth of the slope apron. In this way, we document the filling of healed-slope accommodation by submarine valley systems.

GEOLOGIC SETTING

Auger Basin is approximately 345 km southwest of New Orleans, Louisiana, on the continental slope in the Gulf of Mexico in water depths between 760 and 1220 m (Fig. 2A). It is bounded by tabular salt bodies that are topographically higher than the basin sediments (Fig. 2A). Auger Basin is the central basin in a series of three connected salt-withdrawal mini-basins (Booth et al., 2000). It is separated from Andros Basin to the east by a salt ridge and a down-to-the-east normal fault (East Auger Fault) and is separated from Tampa Basin to the south by a salt ridge (Fig. 2A, B). Exploration in Auger Basin began in the 1980s. The Auger Tension Leg Platform (TLP) was completed in 1994 and was the first in the Gulf of Mexico (McGee et al., 1994). Three fields, Auger, Oregano, and Macaroni (Fig. 2A), produce from the Plio-Pleistocene turbidite reservoirs in Auger Basin.

The Shallow Auger Fan System is a late Pleistocene feature that covers 800 km^2 in Auger and Andros Basins (Winker and Booth, 2000). It was deposited in the western Gulf of Mexico during a time of lowered sea level and extends 112 km from its interpreted source at the Ancestral Mississippi River shelf-edge delta to its termination south of Tampa Basin (Winker and Booth, 2000). The deposits of the Shallow Auger Fan System in Auger Basin are above the final occurrence of the calcareous nannofossil *Pseudoemiliania lacunosa* (0.32 Ma) (Styzen, 1996; Winker and Booth, 2000). The Shallow Auger Fan System onlaps salt to the east and south and is eroded by a large mass-transport complex in the west and north.

The Shallow Auger Fan System is part of the bypass facies assemblage defined by Prather et al. (1998) as occurring above *Discoaster brouweri* (1.84 Ma). This interval is divided into three aprons based on source location (Winker and Booth, 2000) (Fig. 2A, B). Apron 1 is sourced from the southwest and is composed of a ponded apron at the base, the lobe complex, which is subsequently incised by four submarine valley systems (Channels A, B, C, and D; Figs. 2B, 3). Apron 2 is sourced from the northwest and exhibits a compensating geometry with Apron 1 (Winker and Booth, 2000) (Fig. 2A, B). The basal deposits of Apron 2 are thickest in Andros Basin and are ponded against the East Auger Fault (Fig. 2B). The source for Apron 3 is to the northwest, 5 km south of the source for Apron 2 (Fig. 2A, B). North of the East Auger Fault, Apron 3 consists of numerous amalgamated channels that erode into the upper Apron 2 deposits; the channel frequency and the channel incision depth decrease south of the fault. Most of the channels in Apron 3 terminate in a lobe near the sediment exit point of the basin and build a sand-rich ponded apron (Winker and Booth, 2000) (Figs. 2B, 4).

Seismic Data

The seismic data used in this study cover an area of 1200 km^2 and have a bin spacing of 25 m. Using an average sediment velocity of 1915 m/s obtained from the Macaroni M4 well (Fig. 2B) and a peak frequency of 50 Hz for the shallow Auger data, the approximate vertical resolution is 10 m. The data are approximately zero phase (Fig. 4).

Well Data

The Shallow Auger Fan System is penetrated by four wells in Macaroni Field (M1, M3, M3ST1, and M4) and three wells in Oregano Field (OR1, OR2, and OR3) (Fig. 2B). We used checkshot data from the Macaroni M4 well to tie the wells to the seismic data (Fig. 2B). We depth-converted time seismic events using a single average sediment velocity of 1915 m/s that was calculated from the Macaroni and Oregano wells.

APRON 1

Apron 1 covers 250 km^2 of the southern portion of Auger Basin (Fig. 2B). Its sediment was sourced from the west, across the basin-bounding salt ridge (Fig. 2A, B). The deposits are thickest in the west, onlap the basin margin in the south and east, and thin and downlap to the north (Figs. 2B, 3, 4). A series of stacked lobes (lobe complex) are preserved at the base of Apron 1 (Figs. 4, 5, 6). There are no observed channels at this level, but there is considerable postdepositional erosion of the lobe complex by Channels A–C in the channel complex (Figs. 5, 9).

Lobe Complex

The lobe complex is imaged by two negative seismic reflections in the north that increase to a maximum of four reflections

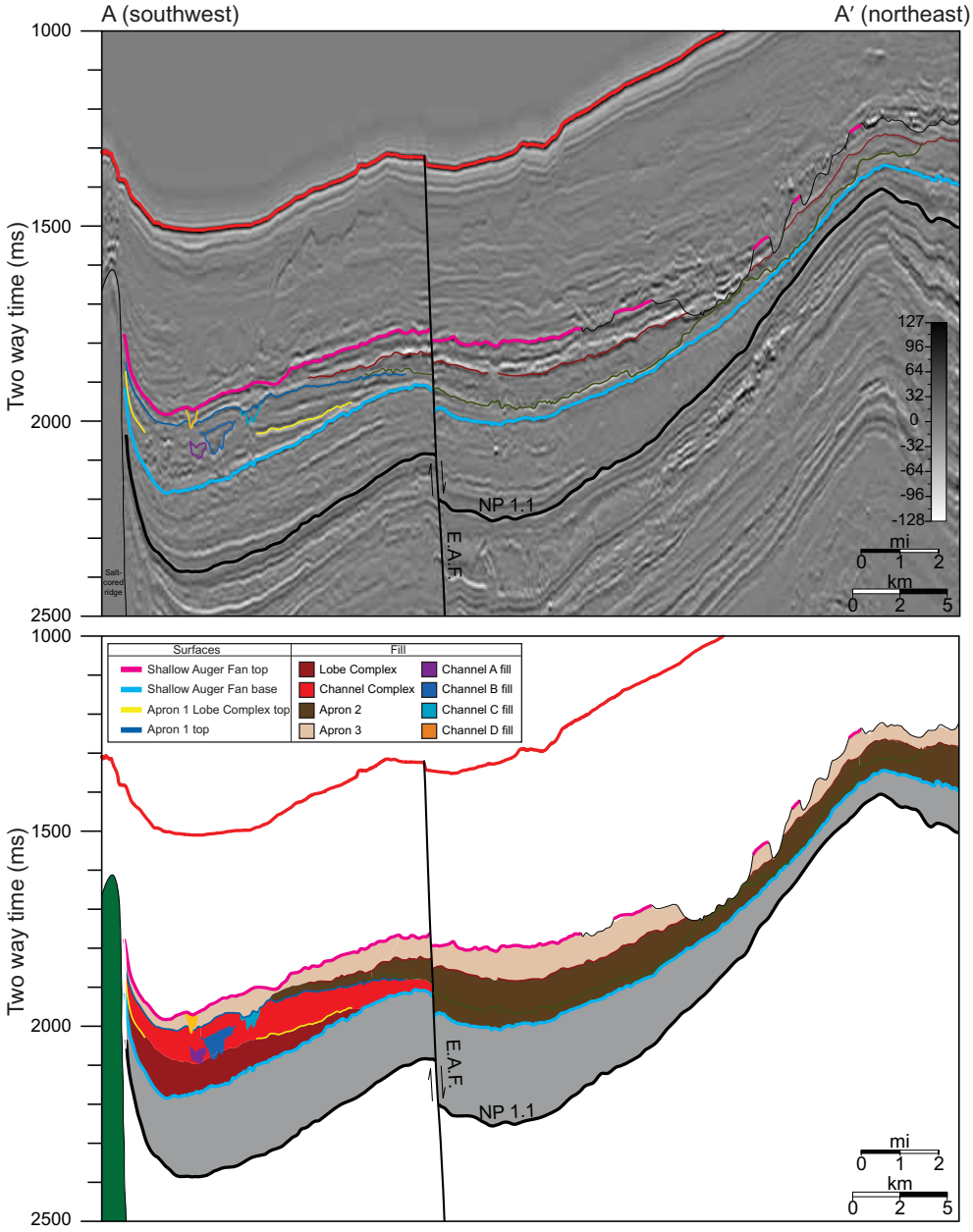

FIG. 3.—Regional seismic section A–A'. The seismic data used in this study cover an area of 1200 km^2 and have a bin spacing of 25 m. Using an average sediment velocity of 1915 m / s obtained from the Macaroni M4 well (Fig. 2B) and a peak frequency of 50 Hz for the shallow Auger data, the approximate vertical resolution is 10 m. The data are approximately zero phase. The location of strike line A–A' is given in Figure 2A. The East Auger Fault (E.A.F.) is a normal fault downthrown to the east. The Shallow Auger Fan System is deposited above a regional datum defined by the last occurrence of a calcareous nannofossil (NP1.1). Apron 1 is sourced from the southwest across the basin margin (Fig. 2A). The lobe complex is the lower ponded deposit at the base of Apron 1 (Fig. 6). Above the lobe complex, the channel complex builds a slope apron at the sediment entry point in the slope healing phase (Fig. 7). It is constructed by Channels A–D (Figs. 8, 9). Seismic image courtesy of CGG Veritas, Houston, Texas.

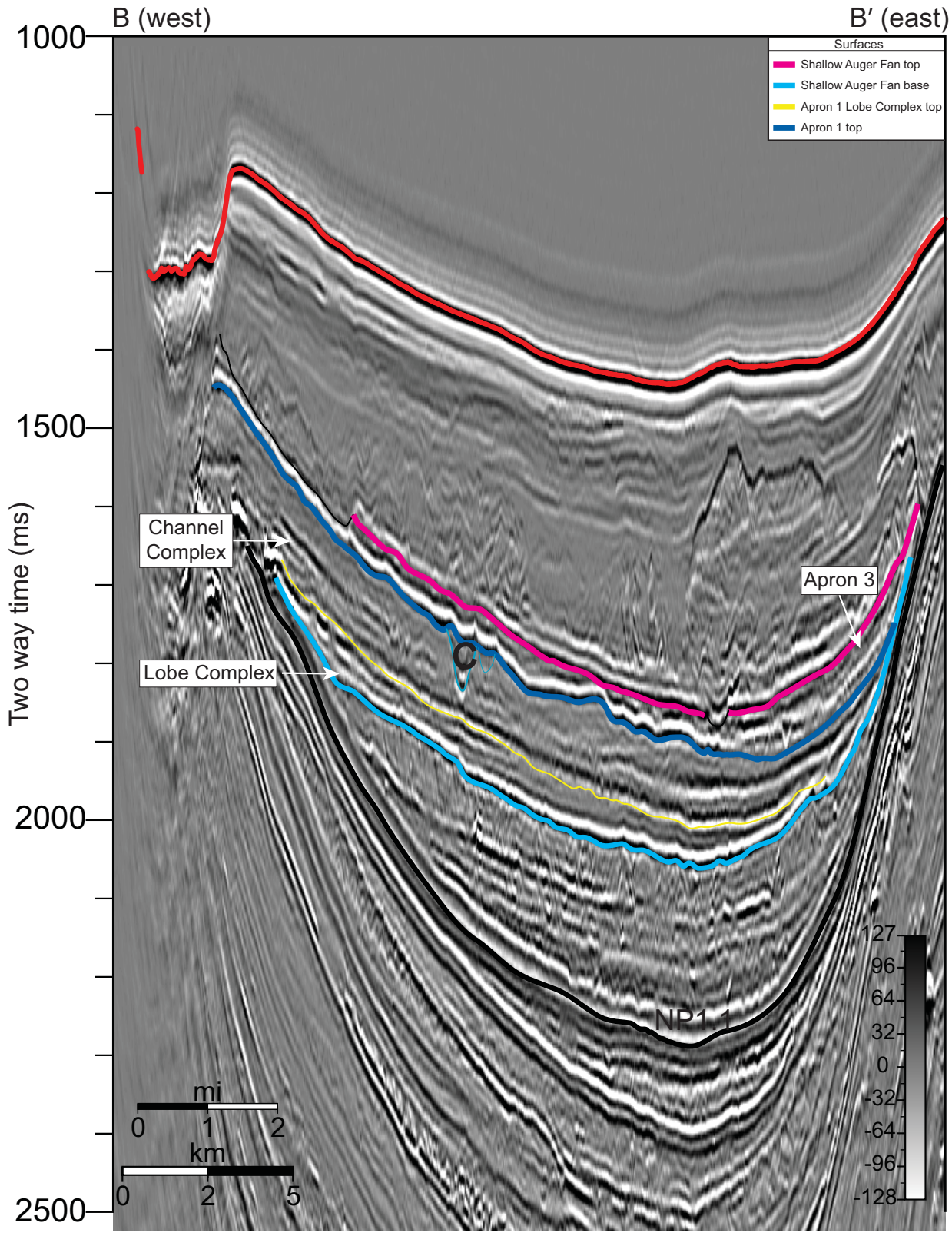

FIG. 4.—Dip seismic line B–B'. The location of dip line B–B' is given in Figure 2A. The section line is oriented along the depositional axis of the lobe imaged in Figure 6. Reflectors within the Lobe Complex are of uniform thickness and continuous across the section; they onlap the basin in the west and east. The channel complex is thickest in the west and thins to the east. Seismic image courtesy of CGGVeritas, Houston, Texas.

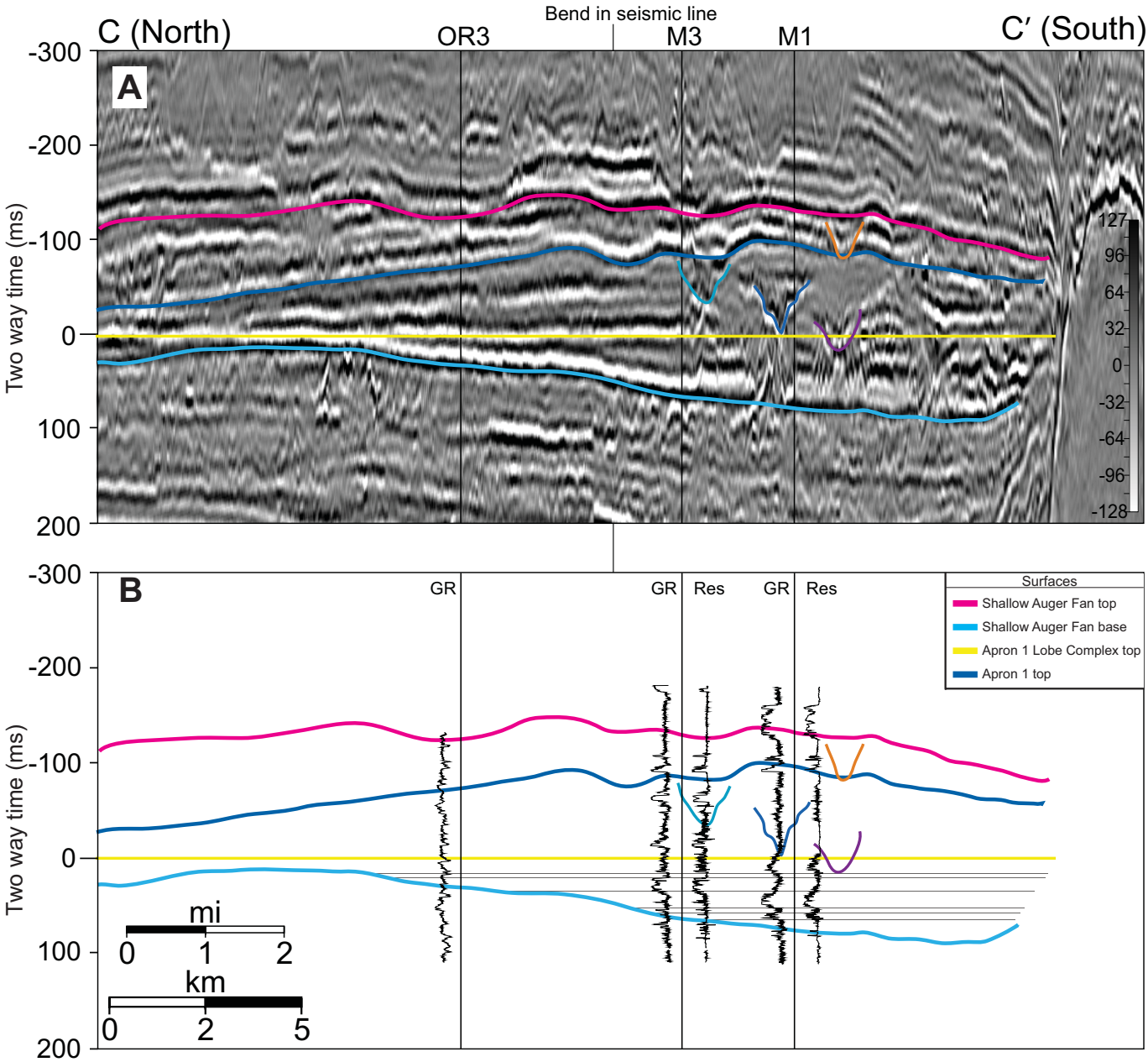

FIG. 5.—Well-log section C–C'. The location of C–C' is given in Figure 2B. The Oregano Wells (OR1, OR2, and OR3) all penetrate the Shallow Auger Fan System at the same location (Fig. 1B); OR3 is shown in the line of section. Similarly, Macaroni wells M3 and M3ST penetrate the Shallow Auger Fan System at the same location; M3 is shown on the plot. To tie the wells to the seismic data, we used checkshot data from the M4 well (Fig. 2B). OR3 and M3 penetrate the lobe complex and the channel complex. The M1 well also penetrates the lobe complex and is the only penetration through a channel; it penetrates a channel form at the top of Channel B (Fig. 8). Seismic image courtesy of CGGVeritas, Houston, Texas.

in the south (Fig. 5). The reflections are continuous and of uniform thickness and amplitude (Fig. 4). The concentric isopach pattern of the lobe complex is slightly elongated toward the sediment entry point in the northwest (Fig. 6). The thickest deposits are in the southeast along the basin margin (Figs. 5, 6). Peak negative amplitudes taken at the top of the lobe complex form a distributary pattern in the north (Fig. 6). The lowest amplitudes (cool colors) are interpreted as slumping associated with the overlying channels (e.g., Fig. 5); the reds and greens in the northern portion of Figure 6 record a single depositional lobe within the lobe complex.

The Macaroni and Oregano wells penetrate the lobe complex along depositional strike (Figs. 5, 6). The Macaroni M1 well penetrates the thickest portion of the lobe complex and contains three thick sandy intervals (Fig. 5). The lower two sand intervals are sharp-based and shale upward, while the upper interval exhibits a gradational base (Fig. 5). To the north, the thickness and number of sandy intervals decreases; this is accompanied by a

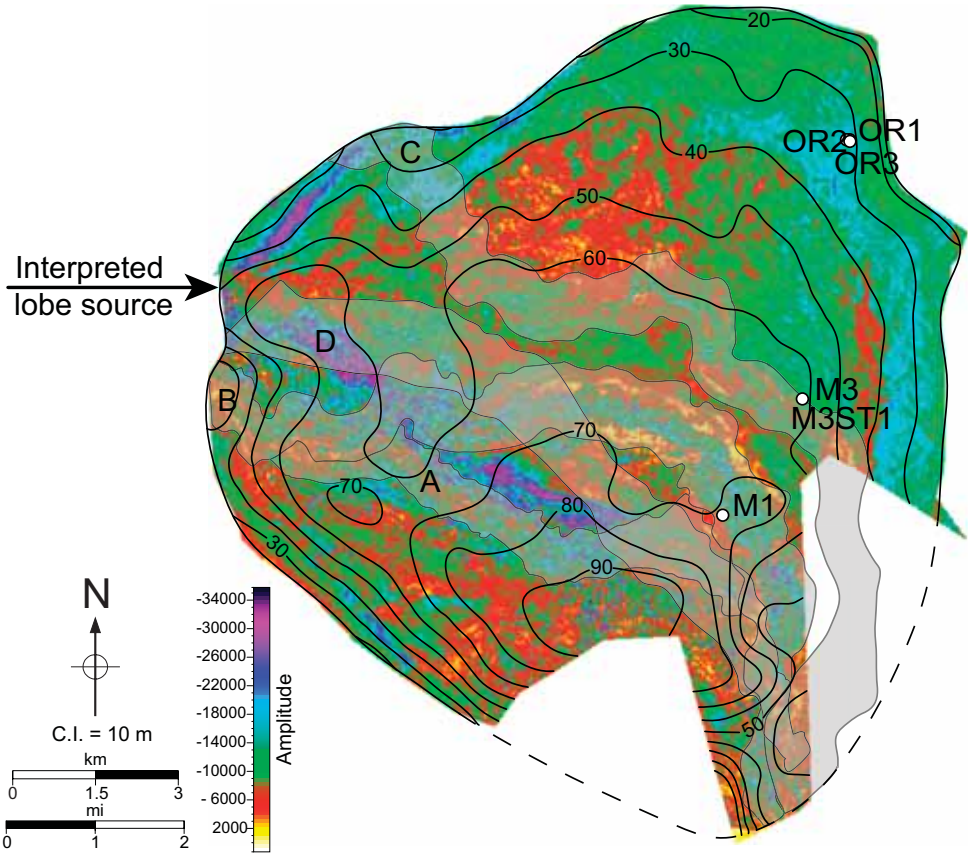

FIG. 6.—Amplitude extraction from the top of the lobe complex. Amplitude extraction from a 25 ms window above and below the top of the lobe complex (yellow line Figures 3, 4, 5, and 9). The contours are isopach thickness of the lobe complex (contour interval is 10 m). The location of Channels A–D are shown in light gray. The highest amplitudes correspond to the high-amplitude reflections at the base of the channels (Figs. 5, 9). The arrow points to the distributary amplitude pattern corresponding to the thick sand within the lobe complex at the Macaroni M3 well (Fig. 5).

decrease in the number of seismic reflections in the lobe complex (Fig. 5). The lower sand content in the Oregano wells relative to the Macaroni M1 and M3 wells is interpreted to record deposition in a more distal position (Figs. 5, 6).

Channel Complex

The top of the channel complex is convex-up along strike and thickest in the west and along the channels (Figs. 5, 7). Individual reflections downlap onto the lobe complex and thin as they onlap the basin margin in the west and east (Fig. 4). Channels A, B, C, and D enter the basin from the west and exit in the south (Figs. 2B, 8). Channels A–C occur at three different stratigraphic levels in the basin and exit the basin at the same height at the downdip sill (Figs. 3, 9). Channel A and Channel B enter the basin at the same position; Channel A is completely truncated by Channel B (Fig. 8). Channel C enters the basin from a source 5.3 km to the north and exits the basin east of Channel B (Figs. 2B, 8). Channel D enters and exits the basin at the same points as Channels A and B, but at a higher position on structure (Fig. 9). Channel D incises into the upper deposits of Apron 1 and Apron 3, suggesting that it postdates the deposition of Apron 3 (Figs. 3, 5, 9).

The channels described in this study are composed of multiple, stacked, channel–levee pairs similar to the channel–levee complexes described by Deptuck et al. (2003) and Barton (this volume). Individual channel forms cannot be traced with confidence in Apron 1. We use the term *channel* to describe a set of channel forms, recognized by basal high-amplitude reflections (HARs of Deptuck et al., 2003). Channels were mapped based on their relative stratigraphic position, sediment source, and, when present, basal high-amplitude reflections (Fig. 9). The channels are characterized by high-angle, high-amplitude reflections (Figs. 5, 9). We interpret these features as rotational slides that developed during prolonged sediment evacuation through the channels. Sawyer et al. (2007) presented a similar interpretation for features below channels in the Mars–Ursa Basin.

We separate the channel complex into two facies. We define the channel facies as the deposits in the interpreted channel margins and the levee facies as all of the deposits outside the channel margins. The seismic characteristics of the channel facies vary for each channel (Figs. 5, 9). Amplitude within a single channel generally decreases with height above the channel base and distance from the sediment entry point (Figs. 5, 9). Individual channel forms in Channel A stack vertically, while the channel forms in Channels B and C shift laterally within the channel margins and are dominated by reincision surfaces at their bases (Fig. 9). Channel D is smaller than the underlying channels and is composed of a single channel form along most of its length (Figs. 5, 9). Channel A incises the upper 20 m of the

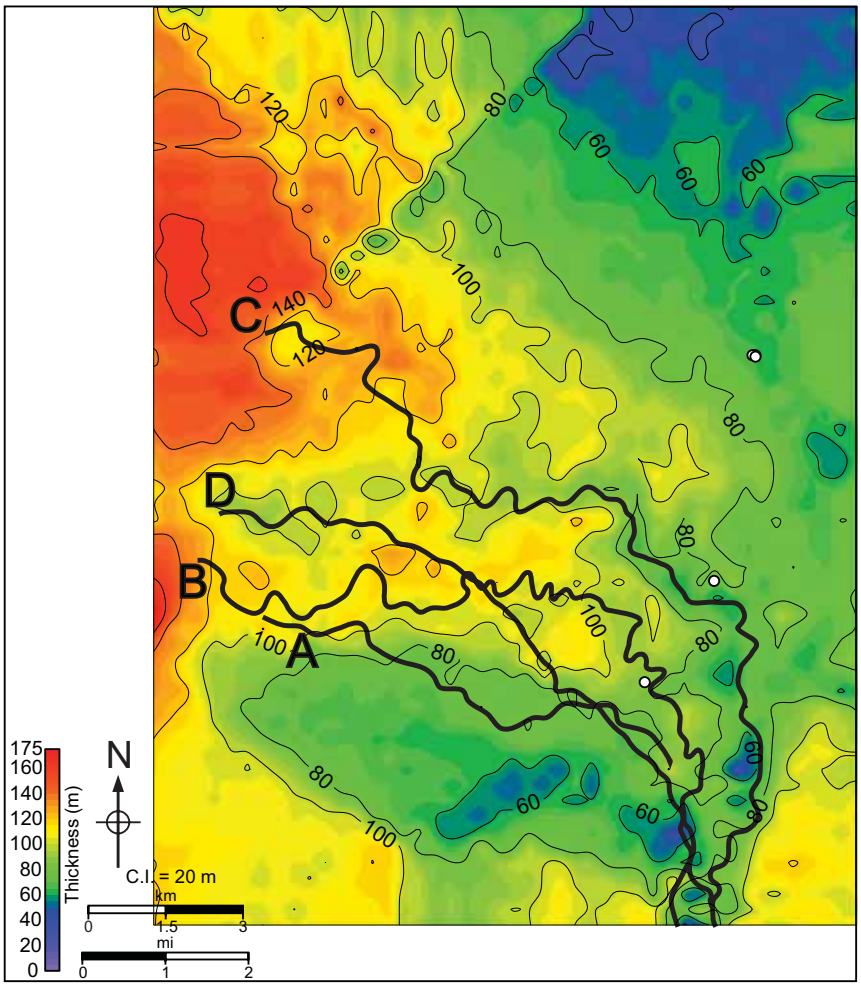

FIG. 7.—Channel-complex isopach. Color and contours are isopach thickness in meters of the channel complex, calculated as the difference between the seismically defined thickness of Apron 1 and the thickness of the lobe complex (Fig. 4). The contour interval is 20 m. The thalweg locations for Channels A–D are indicated with heavy black lines. The channel complex is thickest along the depositional axis of the channels and along the western basin margin.

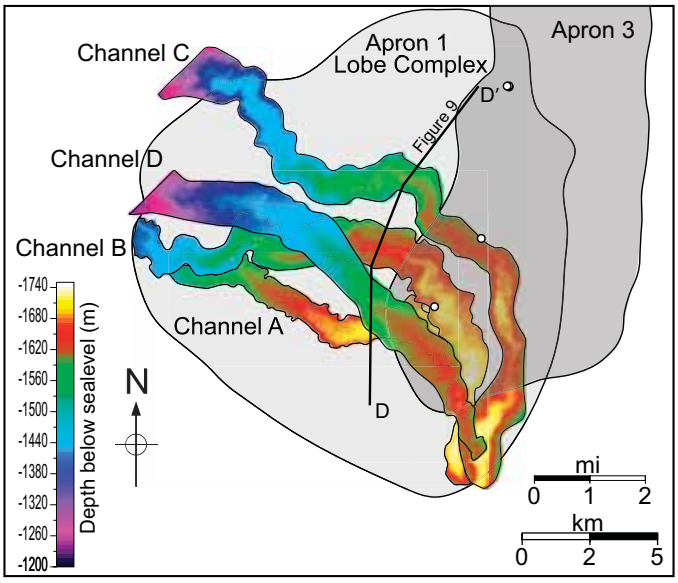

FIG. 8.—Structure map of Channels A–D. Structure map of the channels that cross Apron 1; the colors are meters below sea level converted from two-way travel time using a constant sediment velocity of 1915 m/s. Channels A–C occur within the channel complex at the top of Apron 1; Channel D crosses the top of the channel complex and Apron 3 (Fig. 9). The position of cross section D–D' (Fig. 9) is indicated with a heavy black line. The location of the lobe complex at the base of Apron 1 (Fig. 6) and Apron 3 are shown in light gray (Fig. 2B).

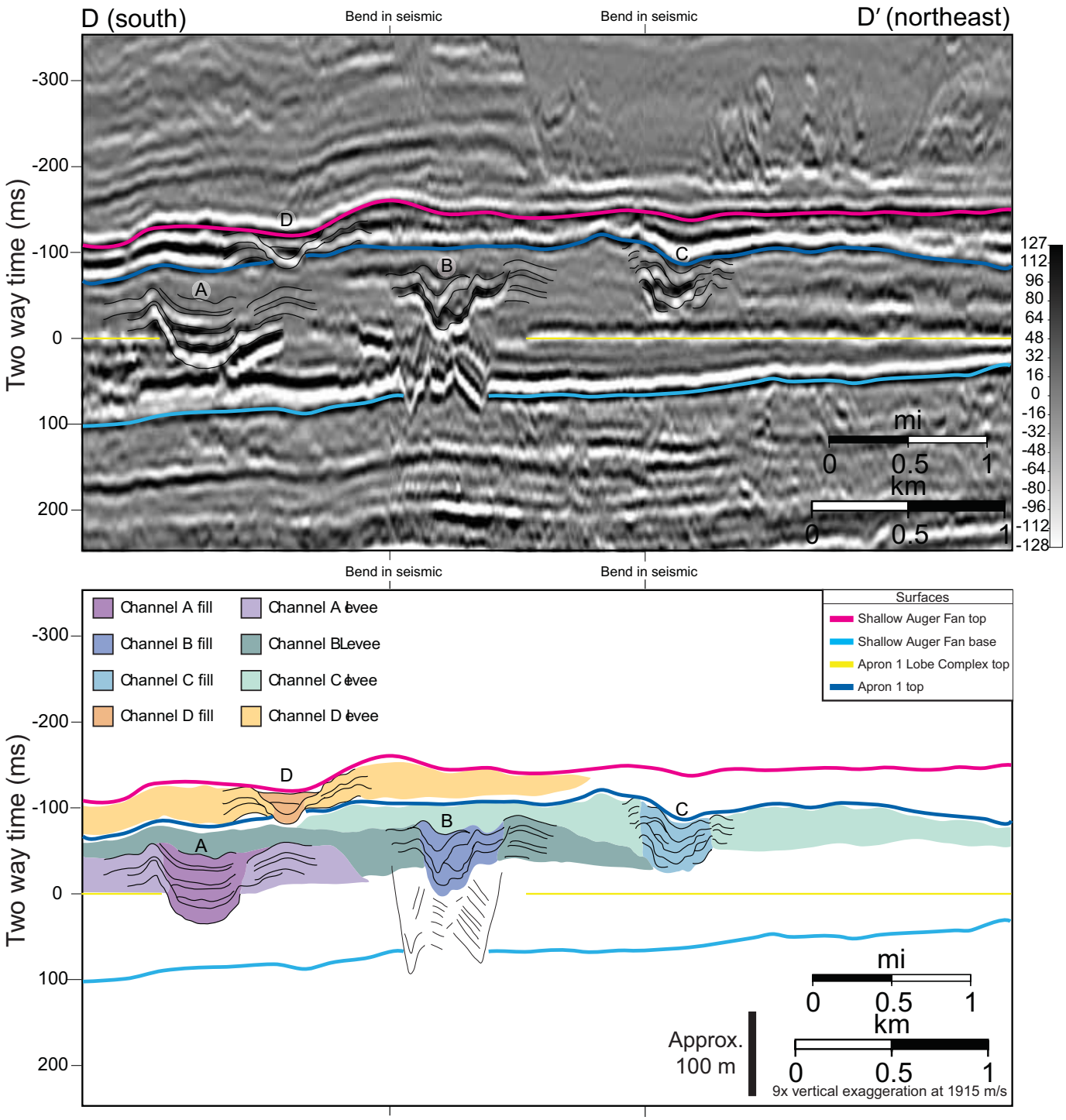

FIG. 9.—Type channel seismic section D–D'. The location of cross section D–D' can be found in Figure 8. The channel complex develops through the deposition of Channels A–D and their associated levees. Note the presence of the high-amplitude reflections below Channel B that deform the underlying deposits of the lobe complex. This section highlights the variability in the stacking patterns that exist between channels. Seismic image courtesy of CGGVeritas, Houston, Texas.

lobe complex, while Channels B and C erode into the levee facies associated with the underlying channels (Figs. 5, 9). Where the channels are proximal to each other, the Levee Facies partially fills the antecedent topography of underlying channels (Fig. 9).

There is variability in the seismic reflections of the levee facies as a function of position (Fig. 10). In cross section, amplitude and continuity in the levee facies decreases away from the channel margins (Figs. 5, 9). The slope of the levees decreases away from the channels and the reflections downlap (Figs. 5, 9).

The nature of the seismic reflections in the study area suggests that the lithology of the channel and levee facies exhibit a high degree of spatial variability.

Well penetrations through the channel facies and the levee facies generally have a lower sand content, and the individual beds are thinner than in the lobe complex (Fig. 5). The Macaroni M1 well is the only penetration through the channel facies (Figs. 5, 8). It penetrates the top of Channel B 11 km from its entry point into the basin and is composed of two thin, sand-poor intervals (Fig. 5). The levee facies is composed of intercalated sand and shale; sand content is greater near the channel margins (Fig. 5).

The top of Apron 1 is draped by a continuous, 6-meter-thick shale interval in all penetrating wells that corresponds to the continuous strong positive reflection at the top of Apron 1 (D seismic facies of Prather et al., 1998) (dark blue line in Figs. 5, 9). We interpret the draping shale as a condensed interval that marks the shift in the locus of deposition to the north and increasing deposition in Apron 2; Channel D occurs above this interval (Figs. 2B, 4, 8).

Channel Morphology

We examined the morphology of the submarine valley systems along their length to better understand how healed-slope accommodation is filled in Auger Basin. Measurements were taken from a series of cross sections that lie perpendicular to the channel margins at approximately 350 m intervals along each of the identified channels (Figs. 8, 10). Measurements of thickness are taken with respect to a datum at the base of the levee facies (dashed line, Fig. 10 inset). The position of the datum coincides with the relative decrease in outer-levee slope away from the channel, which we interpret to be the depositional surface at the base of the channels (Fig. 10). The position of the datum changes for each channel; the datum for Channel A corresponds to the top of the lobe complex.

The measurements taken along the submarine valley systems follow a methodology similar to those detailed in Pirmez and Imran (2003) and Deptuck et al. (2007) for single channel–levee pairs (Fig. 10). We recorded bankfull width (measured between the outer levee margins), thalweg width (the width at the deepest portion of the basal channel form), maximum thickness of levee deposit (from the levee crest to the datum; orientation given is facing in the downstream direction), channel-fill thickness (measured from fill top to the base of the deepest channel-form thalweg), and generated cross sections along the length of each of the channels (Fig. 10 inset; Fig. 11). From these data, we calculated gradient, sinuosity, and the width-to-depth ratio (W/D). In addition to the cross-section measurements, we also measured the wavelength, amplitude, and radius of curvature of the channel meanders.

Channel A.—

Channel A is truncated in both the updip and downdip reaches by Channel B (Fig. 8).

The preserved reach is characterized by low sinuosity, ranging between 1 and 1.25 (Fig. 12). The depth of the channel base below the datum horizon decreases down the length of the preserved reach; this is accompanied by an increase in sinuosity and channel width (Figs. 11, 12). Despite a downdip decrease in the levee deposit thickness, there is an increase in the distance between the top of the channel fill and the levee crest down the channel (Fig. 12).

Channels B and C.—

The morphology of Channels B and C are similar (Fig. 10). They have a higher sinuosity and a lower meander amplitude, wavelength, and radius of curvature than Channel A (Figs. 10, 12; Appendix A). The depth of the channel base below the datum increases down the length of each channel (Fig. 11). For the first 5.5 km of Channel B, the channel base is an average of 5 m below the datum and increases from this point to the end of the channel. The base of Channel C is below the datum horizon down the entire length of the channel, and incision rapidly increases from a distance of 16 km to the basin exit point (Figs. 11, 12). Both channels incise into the lobe complex at their distal ends. The increased incision corresponds to a decrease in levee deposit thickness (Fig. 12). Thalweg and bankfull width and sinuosity also decrease down the length of the channels as incision increases (Fig. 12).

In the proximal regions of Channels B and C, the channel filled from the base of the channel to the levee crests (Fig. 11). Levee deposits are thickest in this region (Fig. 11). In contrast, in the distal channel reaches where the levee deposits are thinner, the top of the channel fill lies below the levee crests (Figs. 9, 11). In the downdip region, the topographic low at Channel B was filled by the overbank deposits of Channel C (Fig. 9). Conversely, Channel C downdip remained a topographic low until it was filled by the onlapping deposits of Apron 3 (Fig. 9).

Channel D.—

Channel D is smaller than Channels A–D and varies less along the length of the channel than the underlying channels (Figs. 10, 11, 12). While there is a slight decrease in the channel width and thickness of the levee deposit, the depth of the channel below the datum and the sinuosity are nearly constant (Fig. 12). Unlike Channels B and C, the channel fill is below the levee crest for the entire length of the channel (Fig. 11).

DISCUSSION

Active channels adjust to an equilibrium profile that is the baselevel surface. Channels either deposit or erode to attain this equilibrium state (Pirmez et al., 2000). Channels A–C in the channel complex are interpreted to record the evolution of channels to an equilibrium profile, and Channel D is interpreted to record a channel that is at the equilibrium profile. Below, we describe the morphologic evolution of channel systems to their equilibrium profile. To gain insight into the growth of the channel complex slope apron and the effects on the morphology of Channels A–D, we first define the surface on which the channel-complex was deposited. The top of the lobe complex is ideal since it was deposited during the ponded phase and should be approximately horizontal (Fig. 1).

Paleotopography of the Channel Complex

To compare the topography, we projected the topography of each channel onto a single cross section (Fig. 13). In this way we compare the channel characteristics at the same position along depositional strike (Fig. 13A). The projection distance for Channels A, B, and D were small (order 1.5 km). The projection distance for Channel C is significantly greater (as much as 4 km) (Fig. 13A).

To account for postdepositional subsidence in the basin, we assume that the top of the lobe complex is a paleo-horizontal

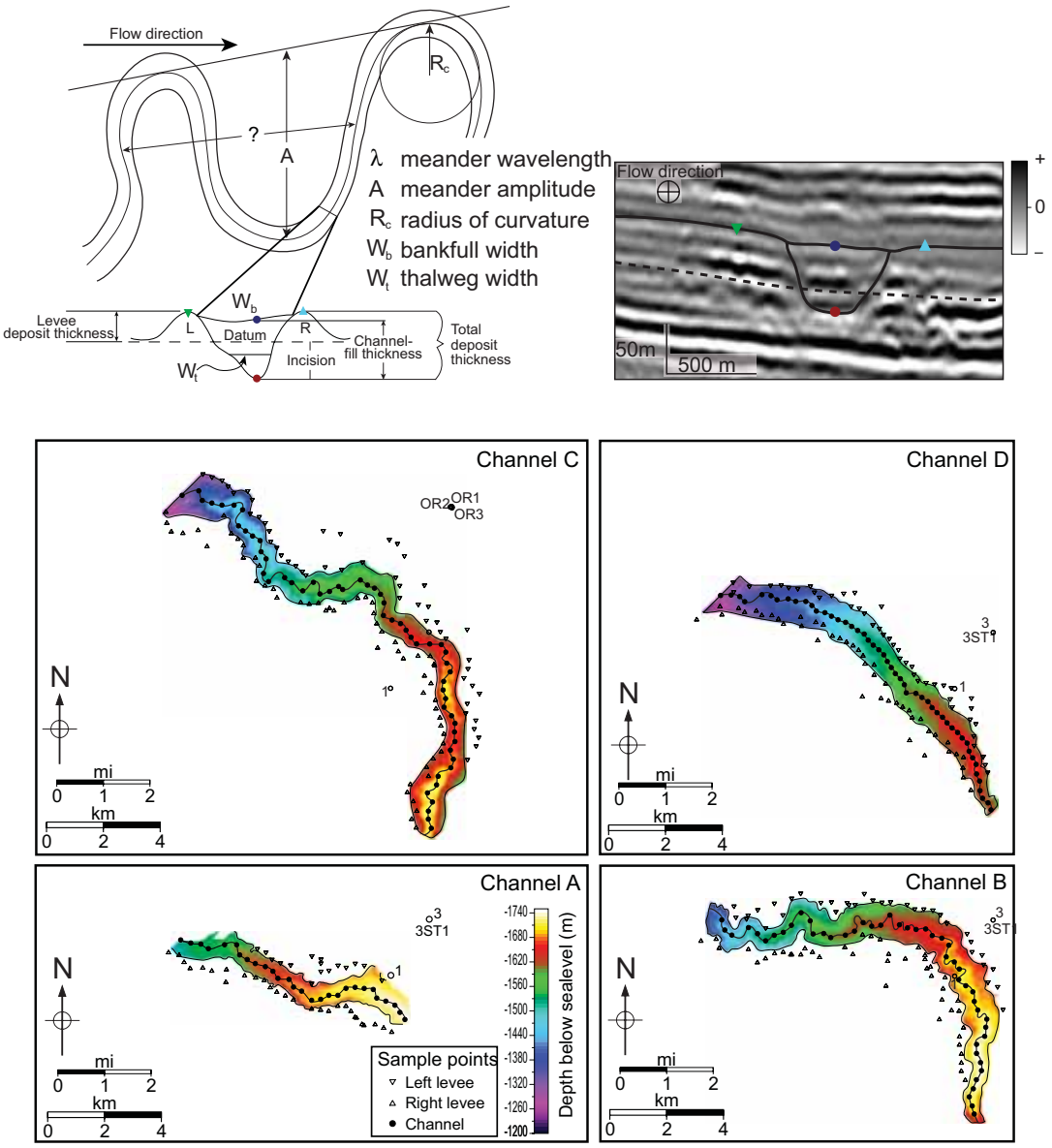

FIG. 10.—Definition of measured channel parameters. A schematic representation of the measurements taken along Channels A–D. The results are presented in Figures 11 and 12. These data are used in the analysis of the channels. The colors and depth conversion technique for the plan-view maps of Channels A–D are the same as in Figure 8. The channels were sampled at approximately 350 m intervals along their length. At each sample point, channel width and depth (circles), and levee deposit thickness (triangles) were extracted. Meander wavelength, amplitude, and radius of curvature are taken from the channel thalweg (heavy black line) and were recorded at the nearest channel sample point. Seismic image courtesy of CGGVeritas, Houston, Texas.

surface (Fig. 1) and we assume no subsidence during deposition of the channel complex (sediment supply >> subsidence). We then flatten the top of the channel fill and the base of each of the overlying channels with respect to this surface to recover the paleotopography of each channel (Figs. 13B, C, 14). When these surfaces are flattened in this manner, the variation in topography is striking: the channel-top gradients remain constant while there is an increase in the channel-base gradients of Channels A–D (Fig. 14A, B). This is perhaps most clear when comparing Channel A and Channel C (Fig. 14A, B).

For each flattened channel, we calculate the average gradients for the projected data (valley gradient) and for the unprojected data (thalweg gradient) (Fig. 15A). To examine changes down the channels, we also calculate the gradients over a 4 km window for the projected data at the tops and bases of the flattened channel surfaces (Fig. 15B). In the calculation of gradient, we exclude the first 5 km and the last 1.5 km of the channel data, where erosion and slumping of the lobe complex leads to irregularities in the flattened channel profiles (Fig. 14).

The average valley gradients are calculated along the red lines in Figure 14A and B. The valley gradients increase from 0.08° at the base of Channel A to 0.26° at the base of Channel C as deposition shifts progressively to the north (Figs. 8, 15A). The valley gradients at the top of the fill in Channels A–C are all

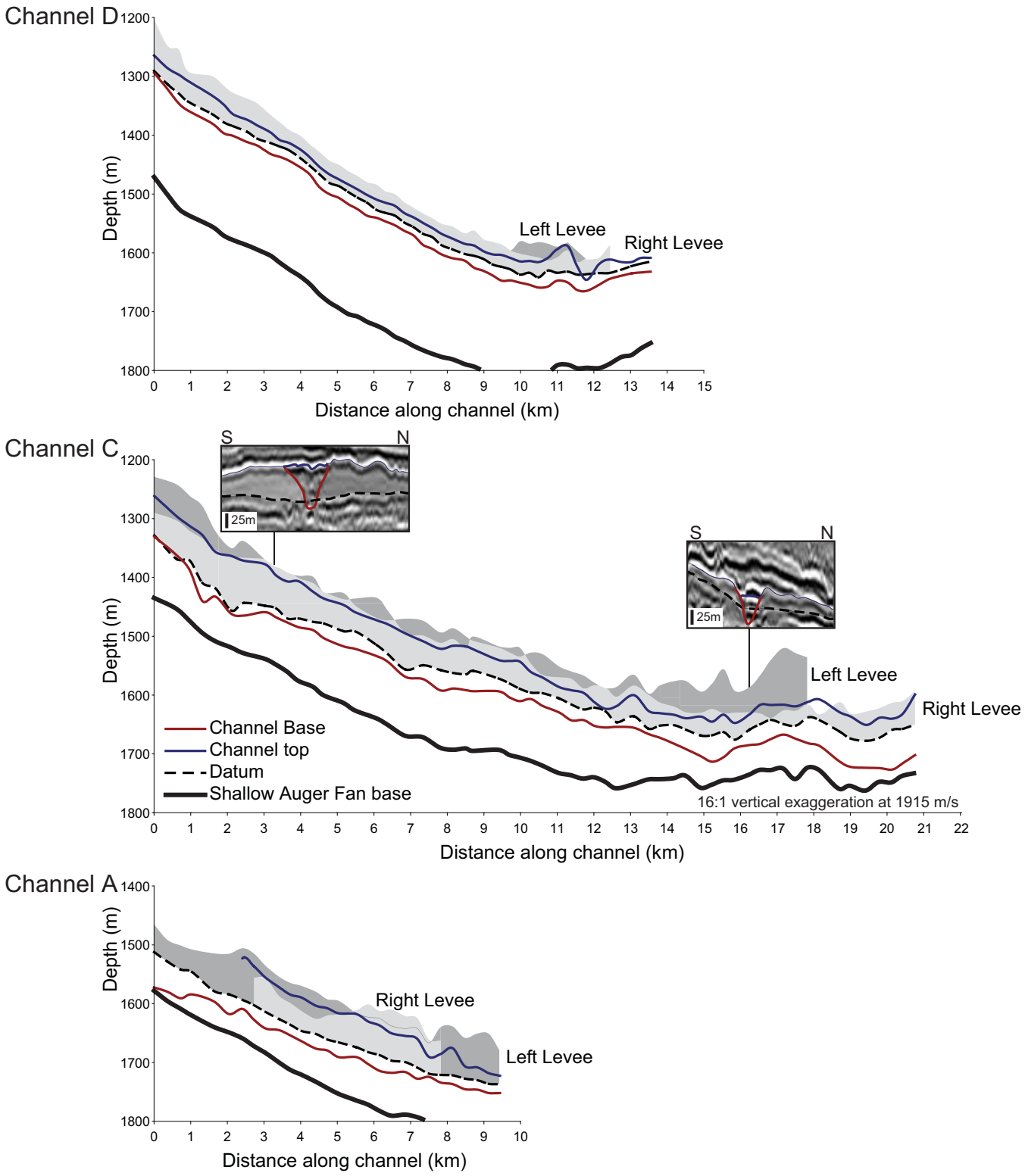

FIG. 11.—Structural profiles along Channels A, C, and D. The profiles are generated from depth-converted two-way-time data extracted from seismically defined horizons at the sample points given in Figure 10. The data were depth converted using a constant sediment velocity of 1915 m / s. Channels B and C are similar; Channel A is truncated by Channel B but is unique because there is an apparent decrease in incision down the channel. Channel D was deposited after the deposition of Apron 3 and shows little change down the length of the channel (Fig. 8). The cross sections of Channel C are at the same vertical exaggeration as the profile and represent the trend of increased incision and decreased levee height downdip that also occurs in Channel B. Seismic image courtesy of CGGVeritas, Houston, Texas.

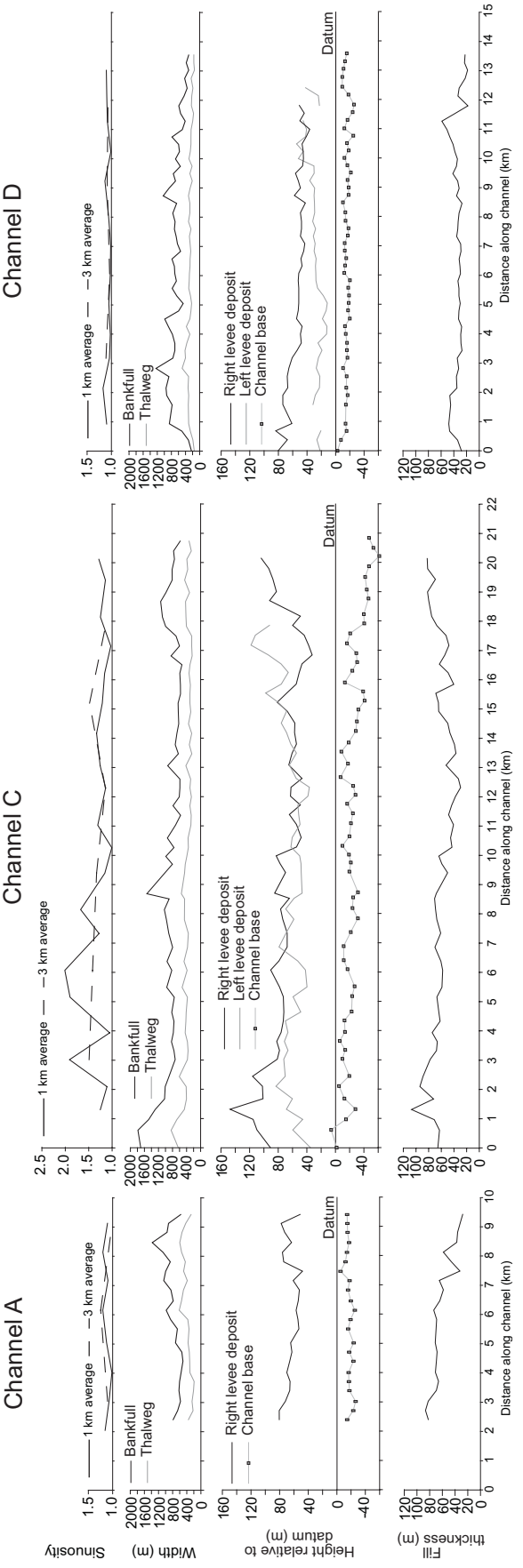

FIG. 12.—Morphologic trends along Channels A, C, and D. Plots of the data collected for Channels A, C, and D extracted from the profiles in Figure 11 at the sample locations indicated in Figure 10. The channel datum corresponds to the position where the slope of the outer levees approaches zero and is interpreted to be the depositional surface at the time the channel was emplaced (dashed line, Figure 10 inset). All measurements of incision and levee height are taken with respect to this datum (Figure 10 inset).

approximately 0.35° (Figs. 14A, 15A). The valley gradients at the top of the channels are interpreted to represent the gradient just before avulsion.

The average thalweg gradients are calculated for the channel bases using the total distance of the sinuous channel thalweg (Fig. 13A). The increase in sinuosity through the deposition of Channels A–C results in thalweg gradients that are lower than the valley gradients, which approach a constant value of 0.08° (Fig. 15A). The thalweg gradients are interpreted to develop as the channels attempt to reach an equilibrium state by either eroding or aggrading to smooth the local topography.

The gradient at the base of Channel D reflects the topography that developed during the deposition of Channels A–C and Apron 3 (Figs. 5, 7, 8). The valley gradient is 0.48°, and the thalweg gradient is slightly lower than the valley gradient at the top of the underlying channels (Fig. 15A). The gradient at top of Channel D is similar to the channel-top gradients of Channels A–C (Fig. 15A).

Depositional Characteristics of the Channel Complex

The healed-slope accommodation in southern Auger Basin is filled by the channel complex. Channel A occurs at the transition between the ponded deposits of the lobe complex and the slope deposits of the channel complex (Fig. 9). Erosion of the proximal and distal portions of Channel A, however, obscures the exact nature of this transition (Fig. 8). The morphology and position of the preserved reach in Channel A is similar to the morphology of the reach between 8 km and 12 km in Channel C (Figs. 8, 10 12). This suggests that the preserved reach is not representative of the overall morphology of the channel. We interpret that prior to removal of the proximal and distal reaches by Channel B, the morphology of Channel A resembled that of Channels B and C.

The incremental growth of the fan and the transition from ponded deposition to bypass is recorded by the increasing valley gradients in Channels A–D (Fig. 15A). This is the result of preferential sedimentation at the basin entry point and erosion at the exit point (Fig. 16). As sediment accumulates at the entry point to the basin, there is a decrease in the proximal reach gradients at the bases of Channels A–C and a straightening of the longitudinal profiles (Figs. 15B, 16).

While there is an increase in the channel-base gradient through the growth of the channel complex, the gradients at the top of the channel fill remain relatively constant (Figs. 14, 15A, 17). The tops of Channels A–C are approximately parallel as presented in the healed-slope accommodation of Fig. 1 (Fig. 14A). The fact that each channel builds to the same grade suggests that the combination of sediment input and the available accommodation fixes the gradient in the healed-slope accommodation in Auger Basin (Figs. 15A, 17). Once this grade is established for a given channel, it seeks a new path through the basin. This results in increasing channel-base gradients in successive channels as the fan grows and fills the accommodation (Fig. 17).

In the proximal reaches, Channels B and C are aggradational and fill to the levee crests (Fig. 16). They are characterized by broad, thick levee deposits and minimal incision (Figs. 11, 16). This is accompanied by increased sinuosity and channel width, which act in tandem to promote overbank deposition and the areal extent of deposition by the channel belt (Figs. 12, 16). Downdip,

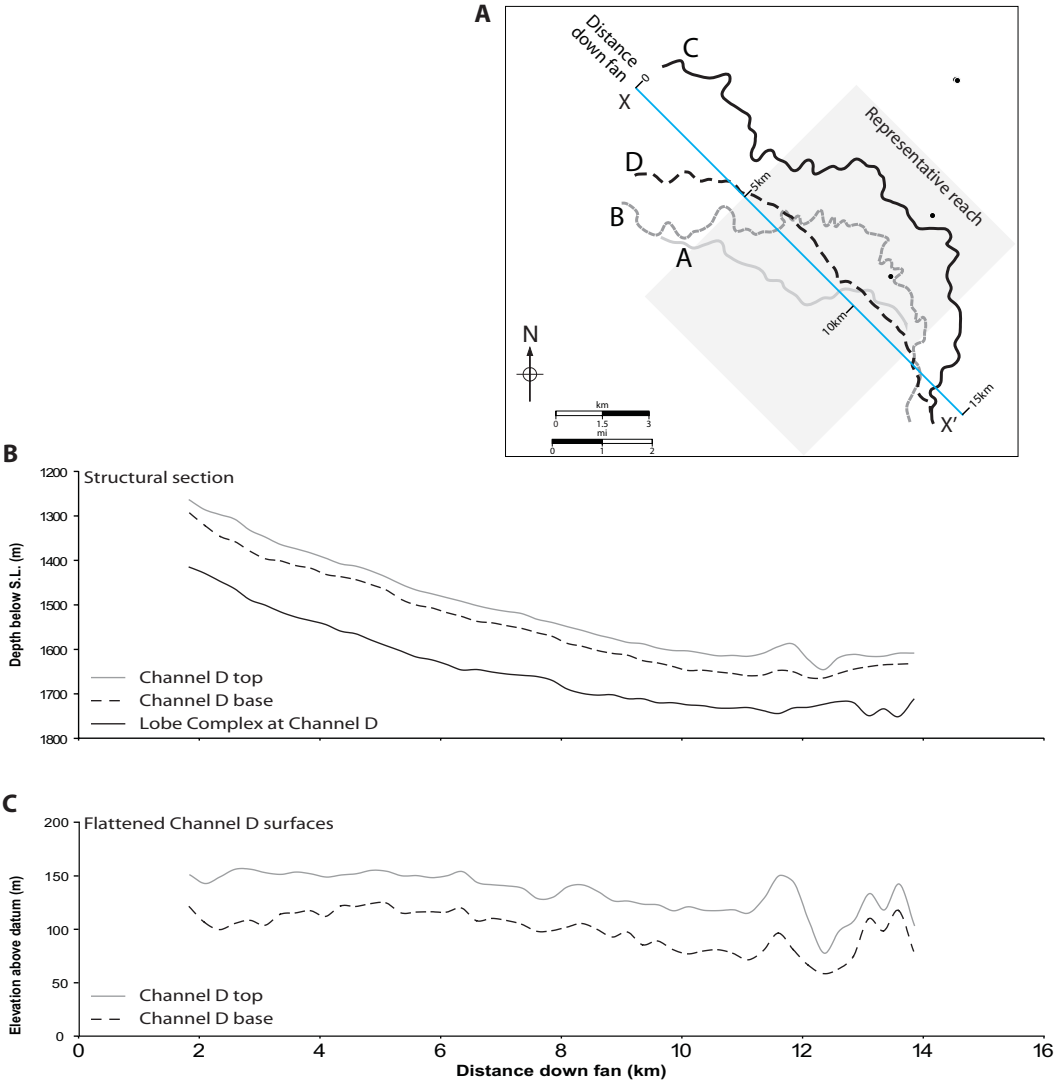

FIG. 13.—Data reprojection and flattening technique. **A)** Sample points for Channels A–D (Fig. 10) projected onto an arbitrary line (light blue line, X–X') through the basin to define "distance down fan" as the distance relative to the first point in Channel C. This coordinate system is used in Figure 14 to compare the channel thalweg gradients of the "representative reach" (gray box). The arbitrary line is 45° west of north and allows us compare samples along strike while minimizing sample-point overlap in sinuous reaches (where a sample farther down the length of the channel would occur before a preceding sample). **B)** The top and base of Channel D and the top of the lobe complex that underlies Channel D are projected onto Line X–X'. **C)** The flattened channel top and base are taken by subtracting the depth of the Channel D surfaces from the depth to the lobe complex. Depth was calculated using a sediment velocity of 1915 m/s.

incision and flow confinement result in a decrease in the concentration of the flow available for levee construction (Figs. 16, 17). As a result, the distal levee deposits are thin (Fig. 16).

Channels A–C record aggradation and build to grade, whereas Channel D represents true bypass. Channel D was deposited following a hiatus during which deposition shifted from the southern source to the north (Fig. 2B). Between the deposition of Channel C and Channel D, the remaining slope accommodation at the basin exit point in Auger Basin was filled by Apron 3 (Fig. 2B) (Winker and Booth, 2000). This explains the relative decrease in the gradients in the distal reach of Channel D and the return to a more convex-up longitudinal profile (Figs. 11, 15B). At this point the system has equilibrated to carry its load across the basin, and flows entering Auger Basin from the northwest are transferred downdip to Tampa Basin.

CONCLUSIONS

Apron 1 in the Shallow Auger Fan System consists of two distinct architectural styles. The lobe complex was deposited in the ponded phase and exhibits characteristics that conform to previous models and observations of low-relief ponded aprons (e.g., Prather et al., 1998). This is followed by deposition of the channel complex in the healing phase, culminating in bypass through Channel D. The healed-slope accommodation fills in the proximal zone through the aggradation of Channels A–C.

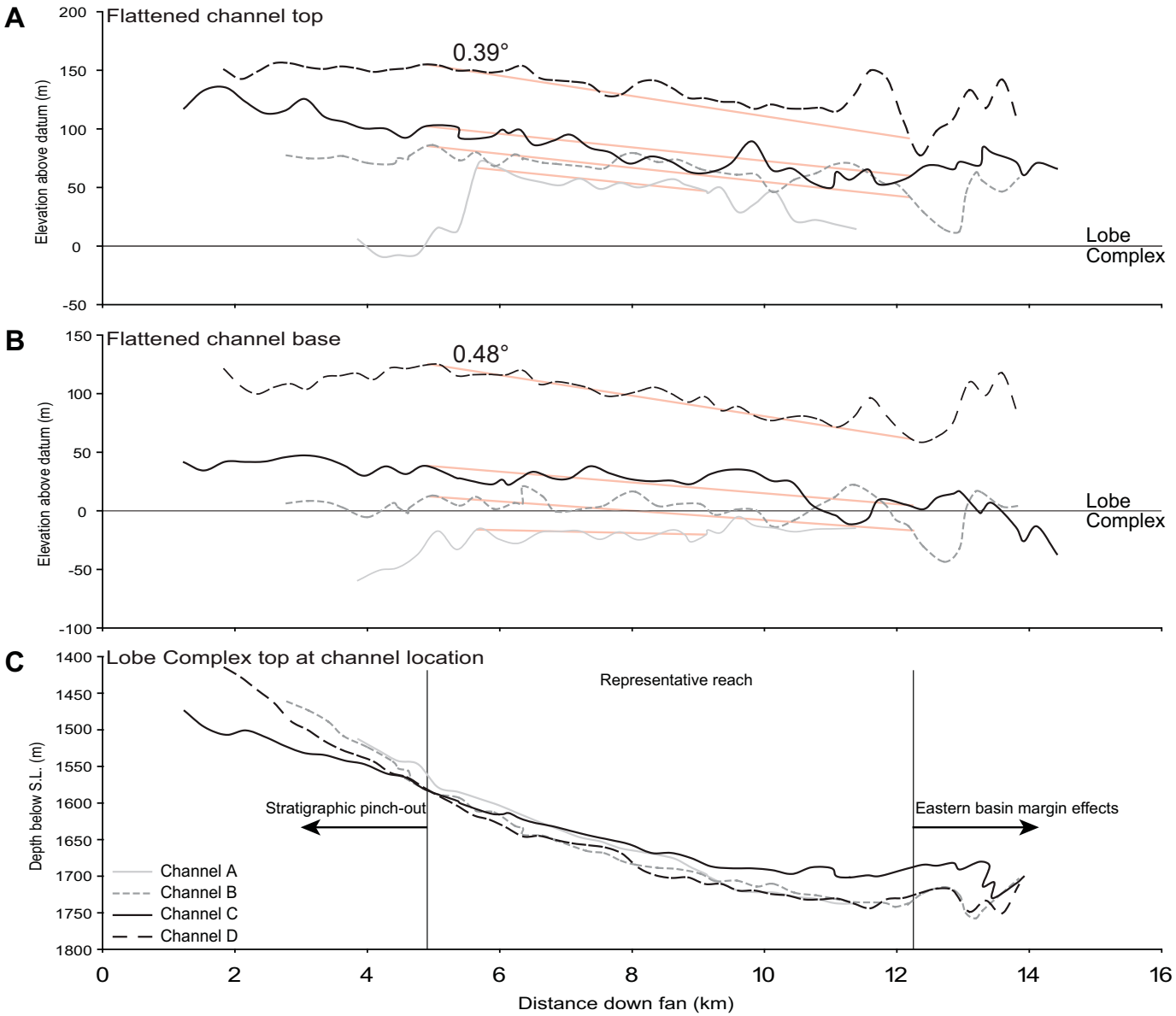

FIG. 14.—Lobe-complex structural profiles and flattened channel profiles. **A)** Channel-top profiles flattened as in Figure 13B and projected onto the arbitrary line given in Figure 13A. The red lines indicate interpreted depositional gradients along the top of Channels A–D and are presented in Figure 15A. **B)** Channel-base profiles plotted as in Part A with the interpreted depositional gradients along the base of the channel shown in red (Fig. 15A). **C)** Profiles of the top of the lobe complex used to flatten the channel surfaces as described in Figure 13. The proximal and distal reaches of the channels are not representative of this channel gradient because of irregularities in the lobe complex. These data are not used in the gradient calculations in Figure 15. Channel A does not extend across the entire representative reach. The downdip point was selected to best match the trends in the other channel profiles. While it is possible that the gradient calculated for Channel A is an underestimate, the difference does not appear to alter the result significantly.

This is recorded by thick levees and low incision depths. Each channel builds until it achieves an along-channel gradient set by a combination of the sediment input and the available accommodation. After this gradient is reached, the channel moves to the north, where there is more accommodation. In addition to controlling channel morphology, the manner in which the healed-slope accommodation fills impacts sand distribution and connectivity.

Through the development of the channel complex, gradients decrease in the proximal reaches of Channels A–C, resulting in increased sinuosity and channel width. This geometry coupled with the break in slope results in preferential deposition at the sediment entry point. Updip, the channels fill to the crest of the thickened levee deposits. This may indicate a higher sand content than observed in the Macaroni M1 well, where the channels remain underfilled. The development of rotational slides or

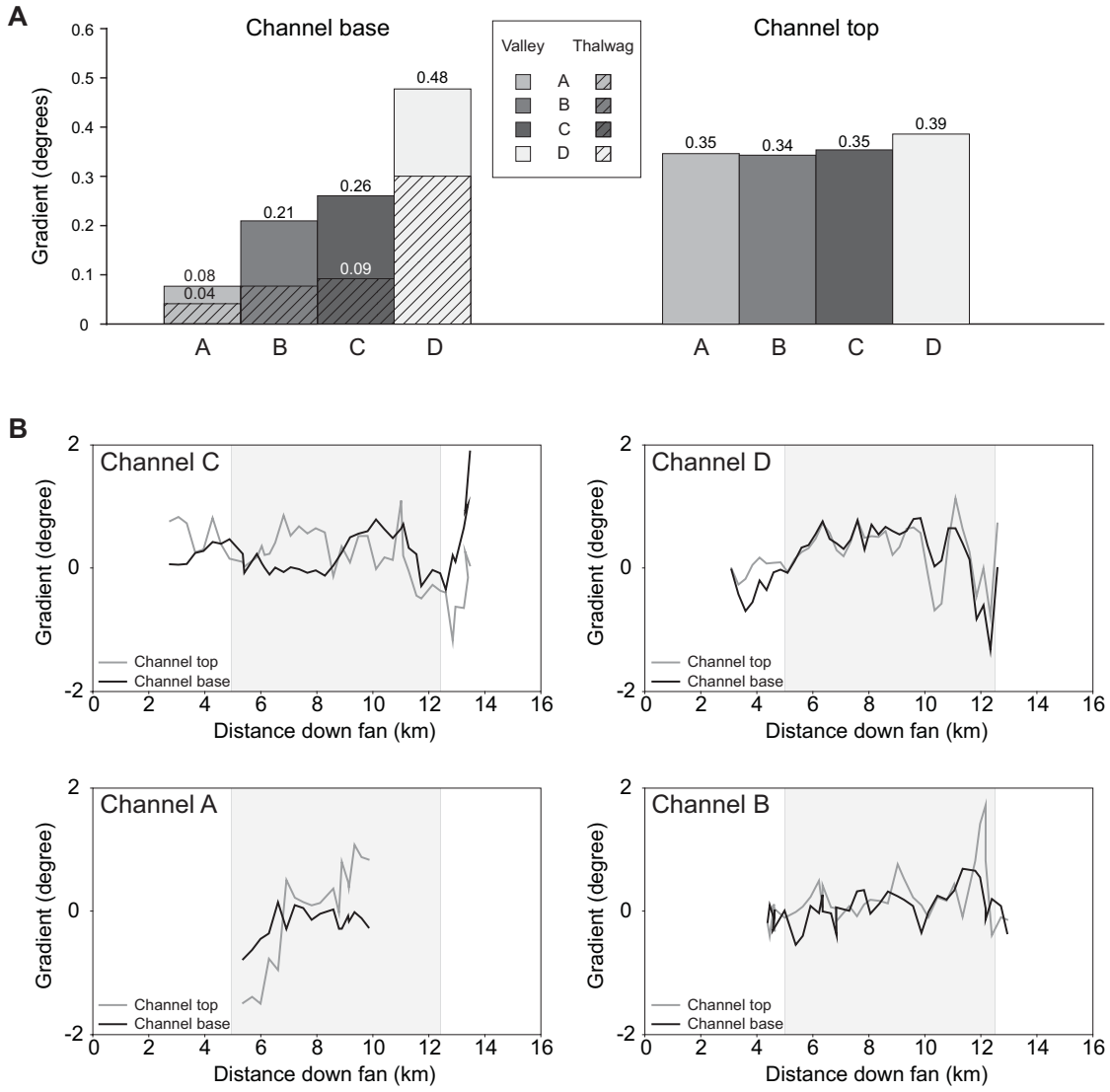

FIG. 15.—Average and instantaneous channel gradients for Channels A–D. **A)** Gradients for Channels A–D calculated for the flattened channel profiles over the "representative reach" defined in Figure 14. The thalweg gradients (hachured area) are calculated using the difference in elevation between the first and last point in the representative reach over the total distance down the channel thalweg. The valley gradients are calculated using the projected distance defined in Figure 13A. **B)** Gradients of the flattened channel profiles calculated as the elevation difference between sample points over the projected "distance down fan" described in 13A. The gradients are averaged over 4 km. The representative reach is indicated by the light gray area.

downcutting caused by increased channel incision downdip may compartmentalize the ponded deposits of the lobe complex.

ACKNOWLEDGMENTS

We thank Shell Exploration and Production Company, Shell Oil, The Shell Foundation, Chevron, and Landmark Graphics for their support. We thank CGGVeritas, Houston, for access to seismic data and Shell for access to seismic and other subsurface data. This research was supported by the Penn State GeoSystems Initiative (Shell and Chevron), the U.T. GeoFluids Consortium, the Kent and Helen Newsham Petroleum GeoSystems Endowment (Penn State), and the Heller GeoSystems Endowment (Penn State). We thank S. Waters, T. Wilson, and B. Bohn from Shell Exploration and Production Company for their support of the graduate program at Penn State. Bill Lyons, Pete Burgess, and Brad Prather provided thoughtful reviews that improved the manuscript. B. Prather, C. Pirmez, M. Harris, and B. Schlotterbeck provided useful insights. Landmark Graphics Seisworks® 3-D, Paradigm Geolog®, and the freeware Generic Mapping Tool program were the primary software tools used in this study.

REFERENCES

ADEOGBA, A.A., MCHARGUE, T.R., AND GRAHAM, S.A., 2005, Transient fan architecture and depositional controls from near-surface 3-D seismic data, Niger Delta continental slope: American Association of Petroleum Geologists, Bulletin, v. 89, p. 627–643.

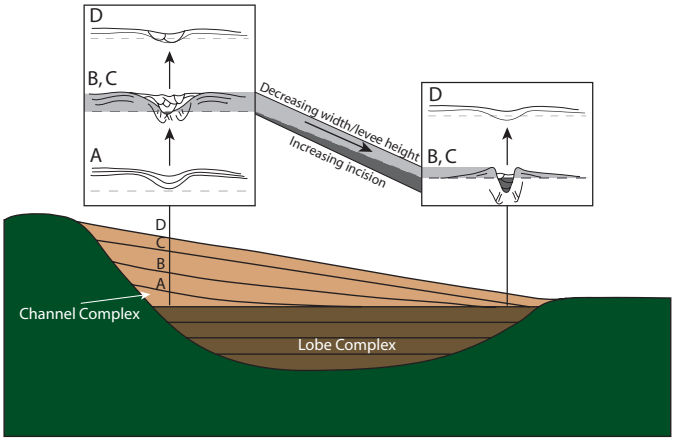

FIG. 16.—Conceptual model for growth of the channel complex. Conceptual model for the growth of the channel complex modified from Figure 1 to reflect the decreasing proximal gradients observed through Channels A–C (black lines in the light brown area). The data suggest that the bases of the early channels are more convex-up than later channels (Fig. 15B). The morphology of Channels B and C offer a mechanism for the growth of the fan; incision is minimal and levee height and channel width are maximum at the sediment entry point (Figs. 11, 12). Incision increases downdip, accompanied by a decrease in levee height and channel width (Fig. 12).

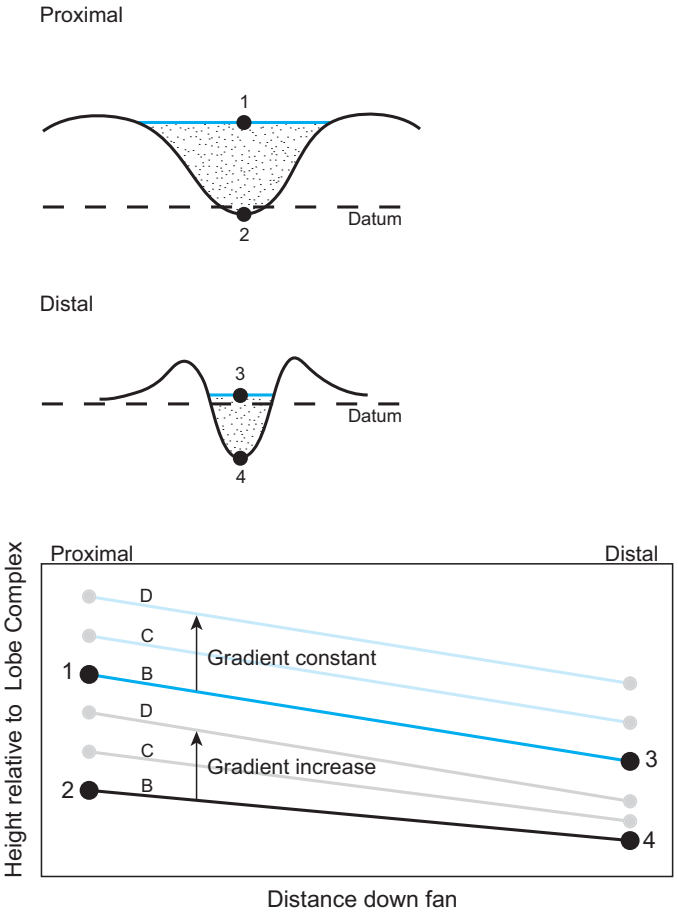

FIG. 17.—Process summary for observed channel morphology and fan growth. Channel profiles are idealized from Figure 11. The along-channel trends are described in the text and in Figure 16. Through the evolution of the channel-complex fan there is an increase in the overall channel-base gradients. The channel-top gradient remains constant and may reflect the balance between sediment input and available accommodation (see discussion in text).

BEAUBOUEF, R.T., AND FRIEDMANN, S.J., 2000, High resolution seismic/sequence stratigraphic framework for the evolution of Pleistocene intra slope basins, western Gulf of Mexico: Depositional models and reservoir analogs: Gulf Coast Section SEPM Foundation, 20th Annual Bob F. Perkins Research Conference, Deep-Water Reservoirs of the World, p. 40–60.

BEAUBOUEF, R.T., ABREU, V., AND ADAIR, N.L., 2003a, Ultra high resolution 3-D characterization of deep-water deposits I: A new approach to understanding the stratigraphic evolution of intra-slope depositional systems: Search and Discovery Article # 40083.

BEAUBOUEF, R.T., VAN WAGONER, J.C., AND ADAIR, N.L., 2003b, Ultra high resolution 3-D characterization of deep-water deposits II: Insights into the evolution of a submarine fan and comparisons with river deltas: Search and Discovery Article # 40084.

BOOTH, J.R., DUVERNAY, A.E., III, PFEIFFER, D.S., AND STYZEN, M.J., 2000, Sequence stratigraphic framework, depositional models, and stacking patterns of ponded and slope fan systems in the Auger Basin: Central Gulf of Mexico slope: Gulf Coast Section SEPM Foundation, 20th Annual Research Conference, Deep-Water Reservoirs of the World, p. 82–103.

BOOTH, J.R., PRATHER, B.E., AND STEFFENS, G.S., 2002, Depositional models for ponded and healed-slope accommodation on above-grade slopes: implications for reservoir characterization (abstract): American Association of Petroleum Geologists, Bulletin, v. 86, p. A20–A21.

BOOTH, J.R., DEAN, M.C., DUVERNAY, A.E., III, AND STYZEN, M.J., 2003, Paleobathymetric controls on the stratigraphic architecture and reservoir development of confined fans in the Auger Basin: central Gulf of Mexico slope: Marine and Petroleum Geology, v. 20, p. 563–586.

DEPTUCK, M.E., STEFFENS, G.S., BARTON, M., AND PIRMEZ, C., 2003, Architecture and evolution of upper fan channel-belts on the Niger Delta slope and in the Arabian Sea: Marine and Petroleum Geology, v. 20, p. 649–676.

DEPTUCK, M.E., SYLVESTER, Z., PIRMEZ, C., AND O'BYRNE, C., 2007, Migration–aggradation history and 3-D seismic geomorphology of submarine channels in the Pleistocene Benin-major Canyon, western Niger Delta slope: Marine and Petroleum Geology, v. 24, p. 406–433.

HOYAL, D.C.J.D., VAN WAGONER, J.C., ADAIR, N.L., DEFFENBAUGH, M., LI, D., SUN, T., HUH, C., AND GIFFIN, D.E., 2003, Sedimentation from jets: A depositional model for clastic deposits of all scales and environments: Search and Discovery Article # 40081.

IMRAN, J., PARKER, G., AND KATOPODES, N., 1998, A numerical model of channel inception on submarine fans: Journal of Geophysical Research, v. 103, p. 1219–1238.

KNELLER, B.C., and McCaffrey. W., 1999, Depositional effects of flow nonuniformity and stratification within turbidity currents approaching a bounding slope: deflection, reflection, and facies variation: Journal of Sedimentary Research, v. 69, p. 980–991.

MCGEE, D.T., BILINSKI, P.W., GARY, P.S., PFEIFFER, D.S., AND SHEIMAN, J.L., 1994, Geologic models and reservoir geometries of Auger Field, deepwater Gulf of Mexico, *in* Weimer, P., Bouma, A.H., and Perkins, B.F., eds., Submarine Fans and Turbidite Systems: SEPM Foundation, Gulf Coast Section, Fifteenth Annual Research Conference, p. 245–256.

MITCHUM, R.M., JR., 1985, Seismic stratigraphic expression of submarine fans, *in* Berg, O.R., and Woolverton, D.G., eds., Seismic Stratigraphy II: An Integrated Approach to Hydrocarbon Exploration: American Association of Petroleum Geologists, Memoir 39, p. 117–136.

NELSON, C.H., 1984, Modern fan morphology, *in* Nelson, C.H., and Nilsen, T.H., eds., Modern and Ancient Deep-Sea Fan Sedimentation: SEPM, Short Course 14, p. 38–71.

NILSEN, T.H., 1990, Case studies of reservoir geometry in turbidite systems, *in* Brown, G.C., Gorsline, D.S., and Schweller, W.J., eds., Deep-Marine Sedimentation: Depositional Models and Case Histories in Hydrocarbon Exploration and Development: Pacific Section SEPM, p. 247–301.

PIRMEZ, C., AND IMRAN, J., 2003, Reconstruction of turbidity currents in Amazon Channel: Marine and Petroleum Geology, v. 20, p. 823–849.

PIRMEZ, C., BEAUBOUEF, R.T., FRIEDMANN, S.J., AND MOHRIG, D.C., 2000, Equilibrium profile and baselevel in submarine channels: examples from Late Pleistocene systems and implications for architecture in deepwater reservoirs, *in* Weimer, P., Slatt, R.M., Coleman, J.H., Rosen, N.C., Nelson, H., Bouma, A.H., Styzen, M.J., and Lawrence, D.T., eds., Deep-Water Reservoirs of the World: Gulf Coast Section SEPM Foundation, 20th Annual Bob F. Perkins Research Conference, p. 782–805.

PRATHER, B.E., 2003, Controls on reservoir distribution, architecture and stratigraphic trapping in slope settings: Marine and Petroleum Geology, v. 20, p. 529–545.

PRATHER, B.E., BOOTH, J.R., STEFFENS, G.S., AND CRAIG, P.A., 1998, Classification, lithologic calibration, and stratigraphic succession of seismic facies of intraslope basins, deep-water Gulf of Mexico; errata: American Association of Petroleum Geologists, Bulletin, v. 82, p. 707R.

RICHARDS, M., AND BOWMAN, M., 1998, Submarine fans and related depositional systems II: variability in reservoir architecture and wireline log character: Marine and Petroleum Geology, v. 15, p. 821–839.

SAWYER, D.E., FLEMINGS, P.B., SHIPP, C., AND WINKER, C., 2007, Seismic geomorphology, lithology, and evolution of the Late Pleistocene Mars–Ursa turbidite mini-basin, Northern Gulf of Mexico: American Association of Petroleum Geologists, Bulletin, v. 91, p. 215–234.

SHANMUGAM, G., AND MOIOLA, R.J., 1985, Submarine fan models: Problems and solutions, *in* Bouma, A.H., Normark, W.R., and Barnes, N.E., eds., Submarine Fans and Related Turbidite Systems: New York, Springer-Verlag, p. 29–34.

SINCLAIR, H.D., AND TOMASSO, M., 2002, Depositional evolution of confined turbidite basins: Journal of Sedimentary Research, v. 72, p. 451–456.

STYZEN, M.J., 1996, A chart in two sheets of the late Cenozoic chronostratigraphy of the Gulf of Mexico SEPM, Gulf Coast Section, Publication GCS407, 2 p.

TONIOLO, H., LAMB, M., AND PARKER, G., 2006a, Depositional turbidity currents in diapiric minibasins on the continental slope: formulation and theory: Journal of Sedimentary Research, v. 76, p. 783–797.

TONIOLO, H., PARKER, G., VOLLER, V., AND BEAUBOUEF, R.T., 2006b, Depositional turbidity currents in diapiric minibasins on the continental slope: Experiments—numerical simulation and upscaling: Journal of Sedimentary Research, v. 76, p. 798–818.

VAN WAGONER, J.C., HOYAL, D.C.J.D., ADAIR, N.L., SUN, T., BEAUBOUEF, R.T., DEFFENAUGH, M., DUNN, P.A., HUH, C., AND LI, D., 2003, Energy dissipation and the fundamental shape of siliciclastic sedimentary bodies: Search and Discovery Article # 40080.

WINKER, C.D., AND BOOTH, J.R., 2000, Sedimentary dynamics of the salt-dominated continental slope, Gulf of Mexico: integration of observations from the seafloor, near-surface, and deep subsurface, *in* Weimer, P., Slatt, R.M., Coleman, J.H., Rosen, N.C., Nelson, H., Bouma, A.H., Styzen, M.J., and Lawrence, D.T., eds., Deep-Water Reservoirs of the World: Gulf Coast Section SEPM Foundation, 20th Annual Bob F. Perkins Research Conference, p. 782–805.